Inorg. Chem. **2002**, *41*, 1177–1183

Hydrothermal Syntheses, Structures, and Properties of the New Uranyl Selenites $Ag_2(UO_2)(SeO_3)_2$, $M[(UO_2)(HSeO_3)(SeO_3)]$ (M = K, Rb, Cs, Tl), and $Pb(UO_2)(SeO_3)_2$

Philip M. Almond and Thomas E. Albrecht-Schmitt*

Department of Chemistry, Auburn University, Auburn, Alabama 36849

Received October 16, 2001

The transition metal, alkali metal, and main group uranyl selenites, $Ag_2(UO_2)(SeO_3)_2$ (**1**), $K[(UO_2)(HSeO_3)(SeO_3)]$ (**2**), $Rb[(UO_2)(HSeO_3)(SeO_3)]$ (**3**), $Cs[(UO_2)(HSeO_3)(SeO_3)]$ (**4**), $Tl[(UO_2)(HSeO_3)(SeO_3)]$ (**5**), and $Pb(UO_2)(SeO_3)_2$ (**6**), have been prepared from the hydrothermal reactions of $AgNO_3$, KCl, RbCl, CsCl, TlCl, or $Pb(NO_3)_2$ with UO_3 and SeO_2 at 180 °C for 3 d. The structures of **1**–**5** contain similar $^2_\infty[(UO_2)(SeO_3)_2]^{2-}$ sheets constructed from pentagonal bipyramidal UO_7 units that are joined by bridging SeO_3^{2-} anions. In **1**, the selenite oxo ligands that are not utilized within the layers coordinate the Ag^+ cations to create a three-dimensional network structure. In **2**–**5**, half of the selenite ligands are monoprotonated to yield a layer composition of $^2_\infty[(UO_2)(HSeO_3)(SeO_3)]^{1-}$, and coordination of the K^+, Rb^+, Cs^+, and Tl^+ cations occurs through long ionic contacts. The structure of **6** contains a uranyl selenite layered substructure that differs substantially from those in **1**–**5** because the selenite anions adopt both bridging and chelating binding modes to the uranyl centers. Furthermore, the Pb^{2+} cations form strong covalent bonds with these anions creating a three-dimensional framework. These cations occur as distorted square pyramidal PbO_5 units with stereochemically active lone pairs of electrons. These polyhedra align along the *c*-axis to create a polar structure. Second-harmonic generation (SHG) measurements revealed a response of 5× α-quartz for **6**. The diffuse reflectance spectrum of **6** shows optical transitions at 330 and 440 nm. The trailing off of the 440 nm transition to longer wavelengths is responsible for the orange coloration of **6**.

Introduction

Recent studies in our group have focused on the preparation of new uranyl iodate compounds with unusual low-dimensional structural motifs. These efforts have resulted in the isolation of compounds such as $UO_2(IO_3)_2$,[1] $UO_2(IO_3)_2(H_2O)$,[1] $A_2[(UO_2)_3(IO_3)_4O_2]$ (A = K,[2] Rb,[3] or Tl[3]), $AE[(UO_2)_2(IO_3)_2O_2](H_2O)$ (AE = Sr,[3] Ba,[2] or Pb[3]), and $Ag_4(UO_2)_4(IO_3)_2(IO_4)_2O_2$, with the latter containing the previously unknown tetraoxoiodate, IO_4^{3-}, trianion.[4] It has become clear during this work that polydentate C_{3v} ligands, such as iodate, provide an excellent platform for building structural versatility into the hydrothermal syntheses of new uranium materials. This is especially true because hexavalent uranium already has a propensity for displaying multiple coordination environments including six-coordinate $[UO_2X_4]^{n-}$ square bipyramids, seven-coordinate $[UO_2X_5]^{n-}$ pentagonal bipyramids, and eight-coordinate $[UO_2X_6]^{n-}$ hexagonal bipyramids.[5–7] Therefore, the combination of the flexibility of these polydentate ligands with U(VI) should lead to a vast array of new compounds from a small subset of reactants. Hence, these studies allow for the further development of the systematics of uranium chemistry[5–8] as well as potential structure−property relationships among solids of similar composition.

On the basis of this information, we have undertaken a study comparing the hydrothermal chemistry of uranyl iodates with that of other U(VI) phases containing trigonal

(1) (a) Bean, A. C.; Peper, S. M.; Albrecht-Schmitt, T. E. *Chem. Mater.* **2001**, *13*, 1266. (b) Weigel, F.; Engelhardt, L. W. H. *J. Less-Common Met.* **1983**, *91*, 339.
(2) Bean, A. C.; Ruf, M.; Albrecht-Schmitt, T. E. *Inorg. Chem.* **2001**, *40*, 3959.
(3) Bean, A. C.; Albrecht-Schmitt, T. E. *J. Solid State Chem.* **2001**, *161*, 416.
(4) Bean, A. C.; Campana, C. F.; Kwon, O.; Albrecht-Schmitt, T. E. *J. Am. Chem. Soc.* **2001**, *123*, 8806.
(5) Burns, P. C.; Ewing, R. C.; Hawthorne, F. C. *Can. Mineral.* **1997**, *35*, 1551.
(6) Burns, P. C. In *Uranium: Mineralogy, Geochemistry and the Environment*; Burns, P. C., Finch, R., Eds.; Mineralogical Society of America: Washington, DC, 1999; Chapter 1.
(7) Burns, P. C.; Miller, M. L.; Ewing, R. C. *Can. Mineral.* **1996**, *34*, 845.
(8) Penneman, R. A.; Ryan, R. R.; Rosenzweig, A. *Struct. Bonding (Berlin)* **1973**, *13*, 1.

10.1021/ic0110732 CCC: $22.00
Published on Web 02/13/2002

pyramidal ligands including selenite and tellurite. A survey of uranium-bearing compounds reveals several solids that also contain the selenite anion.[7] These minerals and mineral-like phases include simple compounds such as $UO_2(SeO_3)$[9] and $UO_2(HSeO_3)_2(H_2O)$,[10] as well as solids where transition metals have been incorporated into one-dimensional uranyl selenite structural motifs such as $Cu_4[(UO_2)(SeO_3)_2](OH)_6$[11] and $Pb_2Cu_5[(UO_2)(SeO_3)_3]_2(OH)_6(H_2O)_2$.[12] These solids display a wide variety of uranium oxide topologies and binding modes for the selenite anion as found in uranyl iodate chemistry.[7] Furthermore, the selenite anion provides several advantages over that of iodate in that it is both a better donor ligand for metals (*vide infra*) and is thermally robust.

An additional feature of the uranyl selenite system is the possibility of preparing new noncentrosymmetric (NCS) phases, because the incorporation of moieties with stereochemically active lone pairs of electrons is well-known to yield NCS structures that are often polar owing to partial or complete alignment of these electrons.[13−25] Thus far, all of the uranyl iodate compounds that we have investigated have been centrosymmetric because of the placement of the linear uranyl dication upon or near centers of inversion or higher symmetry. However, this problem may be resolvable through the incorporation of a second metal center with a nonbonding pair of electrons.[13−16]

Herein, we report the hydrothermal syntheses and structures of six new uranyl selenites, $Ag_2(UO_2)(SeO_3)_2$ (**1**), $K[(UO_2)(HSeO_3)(SeO_3)]$ (**2**), $Rb[(UO_2)(HSeO_3)(SeO_3)]$ (**3**), $Cs[(UO_2)(HSeO_3)(SeO_3)]$ (**4**), $Tl[(UO_2)(HSeO_3)(SeO_3)]$ (**5**), and $Pb(UO_2)(SeO_3)_2$ (**6**). The detailed optical and electronic properties of **6**, which is polar, are also presented. These compounds demonstrate the versatility of the selenite ligand in forming mixed-metal uranium compounds with transition metals, alkali metals, and main group elements.

Experimental Section

Syntheses. UO_3 (99.8%, Alfa-Aesar), SeO_2 (99.4%, Alfa-Aesar), $AgNO_3$ (99.9%, Alfa-Aesar), KCl (Ultrapure, Alfa-Aesar), RbCl (99%, Alfa-Aesar), CsCl (99.999%, Alfa-Aesar), TlCl (99.9%, Alfa-Aesar), and $Pb(NO_3)_2$ (99.994%, Fisher) were used as received. Distilled and Millipore filtered water was used in all reactions. The resistance of the water was 18.2 MΩ. The PTFE liners used in these reactions were heated with distilled and Millipore filtered water at 200 °C for 3 d prior to use. *While the UO_3 contains depleted U, standard precautions for handling radioactive materials should be followed. Old sources of depleted U should not be used, as the daughter elements of natural decay are highly radioactive and present serious health risks.*[26] SEM/EDX analyses were performed using a JEOL 840/Link Isis instrument. IR spectra were collected on a Nicolet 5PC FT-IR spectrometer from KBr pellets.

$Ag_2(UO_2)(SeO_3)_2$ (1). UO_3 (253 mg, 0.885 mmol), SeO_2 (196 mg, 1.767 mmol), and $AgNO_3$ (301 mg, 1.767 mmol) were loaded in a 23-mL PTFE-lined autoclave. Water (1.5 mL) was then added to the solids. The autoclave was sealed and placed in a box furnace and heated to 180 °C. After 72 h, the furnace was cooled at 9 °C/h to 23 °C. The product consisted of a pale yellow solution over dark yellow prisms of **1** and yellow needles of $UO_2(SeO_3)$. The mother liquor was decanted from the crystals, which were then washed with water and methanol and allowed to dry. Crystals of **1** were manually separated from $UO_2(SeO_3)$. Yield, 304 mg (46% yield based on U). EDX analysis for $Ag_2(UO_2)(SeO_3)_2$ provided a Ag/U/Se ratio of 2:1:2. IR (KBr, cm^{-1}): ν(U═O, U−O, and Se═O) 883 (s), 831(m, sh), 815 (s), 731(s, sh), 689 (s).

$K[(UO_2)(HSeO_3)(SeO_3)]$ (2). UO_3 (327 mg, 1.143 mmol), SeO_2 (253 mg, 2.287 mmol), and KCl (170 mg, 2.287 mmol) were loaded in a 23-mL PTFE-lined autoclave. Water (1.5 mL) was then added to the solids. The autoclave was sealed and placed in a box furnace and heated to 180 °C. After 72 h, the furnace was cooled at 9 °C/h to 23 °C. The product consisted of a pale yellow solution over bright yellow prisms of **2**. The mother liquor was decanted from the crystals, which were then washed with water and methanol and allowed to dry. Yield, 550 mg (88% yield based on U). EDX analysis for $K[(UO_2)(HSeO_3)(SeO_3)]$ provided a K/U/Se ratio of 1:1:2. IR (KBr, cm^{-1}): ν(U═O, U−O, and Se═O) 899 (s), 873 (m, sh), 840 (m), 806 (m), 778 (s), 757 (s, sh), 760 (s, br), 661 (s).

$Rb[(UO_2)(HSeO_3)(SeO_3)]$ (3). UO_3 (242 mg, 0.846 mmol), SeO_2 (222 mg, 1.692 mmol), and RbCl (242 mg, 1.692 mmol) were loaded in a 23-mL PTFE-lined autoclave. Water (1.5 mL) was then added to the solids. The autoclave was sealed and placed in a box furnace and heated to 180 °C. After 72 h, the furnace was cooled at 9 °C/h to 23 °C. The product consisted of a pale yellow solution over bright yellow needles of **3**. The mother liquor was decanted from the crystals, which were then washed with water and methanol and allowed to dry. Yield, 493 mg (96% yield based on U). EDX analysis for $Rb[(UO_2)(HSeO_3)(SeO_3)]$ provided a Rb/U/Se ratio of 1:1:2. IR (KBr, cm^{-1}): ν(U═O, U−O, Se═O) 902 (s), 877 (m, sh), 844 (m), 808 (m, sh), 778 (s), 717 (s, sh), 707 (s), 657 (m).

$Cs[(UO_2)(HSeO_3)(SeO_3)]$ (4). UO_3 (254 mg, 0.888 mmol), SeO_2 (197 mg, 1.776 mmol), and CsCl (299 mg, 1.776 mmol) were loaded in a 23-mL PTFE-lined autoclave. Water (1.5 mL) was then added to the solids. The autoclave was sealed and placed in a box furnace and heated to 180 °C. After 72 h, the furnace was cooled at 9 °C/h to 23 °C. The product consisted of a pale yellow solution over yellow needles of **4**. The mother liquor was decanted from the crystals, which were then washed with water and methanol and allowed to dry. Yield, 341 mg (58% yield based on U). EDX analysis for $Cs[(UO_2)(HSeO_3)(SeO_3)]$ provided a Cs/U/Se ratio of

(9) Loopstra, B. O.; Brandenburg, N. P. *Acta Crystallogr.* **1978**, *B34*, 1335.
(10) Mistryukov, V. E.; Michailov, Y. N. *Koord. Khim.* **1983**, *9*, 97.
(11) Ginderow, D.; Cesbron, F. *Acta Crystallogr.* **1983**, *C39*, 1605.
(12) Ginderow, D.; Cesbron, F. *Acta Crystallogr.* **1983**, *C39*, 824.
(13) Halasyamani, P. S.; O'Hare, D. *Chem. Mater.* **1998**, *10*, 646.
(14) Halasyamani, P. S.; O'Hare, D. *Inorg. Chem.* **1997**, *36*, 6409.
(15) Porter, Y.; Bhuvanesh, N. S. P.; Halasyamani, P. S. *Inorg. Chem.* **2001**, *40*, 1172.
(16) Porter, Y.; Ok, K. M.; Bhuvanesh, N. S. P.; Halasyamani, P. S. *Chem. Mater.* **2001**, *13*, 1910.
(17) Harrison, W. T. A.; Dussack, L. L.; Jacobson, A. J. *J. Solid State Chem.* **1996**, *125*, 234.
(18) Harrison, W. T. A.; Dussack, L. L.; Jacobson, A. J. *Inorg. Chem.* **1994**, *33*, 6043.
(19) Dussack, L. L.; Harrison, W. T. A.; Jacobson, A. J. *Mater. Res. Bull.* **1996**, *31*, 249.
(20) Svenson, C.; Abrahams, S. C.; Bernstein, J. L. *J. Solid State Chem.* **1981**, *36*, 195.
(21) Liminga, R.; Abrahams, S. C.; Bernstein, J. L. *J. Chem. Phys.* **1975**, *62*, 755.
(22) Nassau, K.; Shiever, J. W.; Prescott, B. E. *J. Solid State Chem.* **1975**, *14*, 122.
(23) Abrahams, S. C.; Bernstein, J. L.; Nassau, K. *J. Solid State Chem.* **1977**, *22*, 243.
(24) Gupta, P. K. S.; Ammon, H. L.; Abrahams, S. C. *Acta Crystallogr.* **1989**, *C45*, 175.
(25) Bergman, J. G., Jr.; Boyd, G. D.; Ashkin, A.; Kurtz, S. K. *J. Appl. Phys.* **1969**, *70*, 2860.

(26) *In our laboratory, uranium starting materials are stored in a glovebox until needed. All manipulations are carried out wearing a beta torso shield, gloves, and eye protection. All products are stored in a fume hood solely designated for radioactive materials.*

Table 1. Crystallographic Data for $Ag_2(UO_2)(SeO_3)_2$ (**1**), $K[(UO_2)(HSeO_3)(SeO_3)]$ (**2**), $Rb[(UO_2)(HSeO_3)(SeO_3)]$ (**3**), $Cs[(UO_2)(HSeO_3)(SeO_3)]$ (**4**), $Tl[(UO_2)(HSeO_3)(SeO_3)]$ (**5**), and $Pb(UO_2)(SeO_3)_2$ (**6**)

formula	**1-Ag**	**2-K**	**3-Rb**	**4-Cs**	**5-Tl**	**6-Pb**
formula mass	739.69	564.06	610.43	657.87	729.33	731.14
space group	$P2_1/n$ (No. 14)	$P2_1/n$ (No. 14)	$P2_1/n$ (No. 14)	$P2_1/c$ (No. 14)	$P2_1/n$ (No. 14)	$Pmc2_1$ (No. 26)
a (Å)	5.8555(6)	8.4164(4)	8.4167(5)	13.8529(7)	8.364(3)	11.9911(7)
b (Å)	6.5051(7)	10.1435(5)	10.2581(6)	10.6153(6)	10.346(4)	5.7814(3)
c (Å)	21.164(2)	9.6913(5)	9.8542(5)	12.5921(7)	9.834(4)	11.2525(6)
α (deg)	90	90	90	90	90	90
β (deg)	96.796(2)	97.556(1)	96.825(1)	101.0940	97.269(8)	90
γ (deg)	90	90	90	90	90	90
V (Å^3)	800.5(1)	820.18(7)	844.78(8)	1817.1(2)	844.1(6)	780.08(7)
Z	4	4	4	8	4	4
T (°C)	20	−80	−80	20	20	20
λ (Å)	0.71073	0.71073	0.71073	0.71073	0.71073	0.71073
ρ_{calcd} (g cm^{-3})	6.138	4.568	4.792	4.802	5.739	6.225
μ(Mo Kα) (cm^{-1})	341.29	291.79	335.62	298.32	468.55	516.25
$R(F)^a$	0.0526	0.0274	0.0286	0.0241	0.0222	0.0193
$R_w(F_o^2)^b$	0.1347	0.0603	0.0748	0.0627	0.0511	0.0514

^{a} $R(F) = \sum||F_o| - |F_c||/\sum|F_o|$. ^{b} $R_w(F_o^2) = [\sum[w(F_o^2 - F_c^2)^2]/\sum wF_o^4]^{1/2}$.

1:1:2. IR (KBr, cm^{-1}): ν(U═O, U−O, Se═O) 901 (s), 888 (m, sh), 839 (m), 825 (m, sh), 778 (s), 746 (s, sh), 705 (s), 633 (m).

$Tl[(UO_2)(HSeO_3)(SeO_3)]$ (5). UO_3 (217 mg, 0.759 mmol), SeO_2 (169 mg, 1.517 mmol), and TlCl (364 mg, 1.517 mmol) were loaded in a 23-mL PTFE-lined autoclave. Water (1.5 mL) was then added to the solids. The autoclave was sealed and placed in a box furnace and heated to 180 °C. After 72 h, the furnace was cooled at 9 °C/h to 23 °C. The product consisted of a pale yellow solution over bright yellow needles of **5**. The mother liquor was decanted from the crystals, which were then washed with water and methanol and allowed to dry. Yield, 554 mg (quantitative yield based on U). EDX analysis for $Tl[(UO_2)(HSeO_3)(SeO_3)]$ provided a Tl/U/Se ratio of 1:1:2. IR (KBr, cm^{-1}): ν(U═O, U−O, Se═O) 894 (s), 872 (s, sh), 836 (m, sh), 804 (m, sh), 757 (s), 705 (s), 657 (s).

$Pb(UO_2)(SeO_3)_2$ (6). UO_3 (367 mg, 1.283 mmol), SeO_2 (285 mg, 2.566 mmol), and $Pb(NO_3)_2$ (849 mg, 2.566 mmol) were loaded in a 23-mL PTFE-lined autoclave. Water (3 mL) was then added to the solids. The autoclave was sealed and placed in a box furnace and heated to 180 °C. After 72 h, the furnace was cooled at 9 °C/h to 23 °C. The product consisted of a pale yellow solution over large clusters of orange prisms of **6** and yellow needles of $UO_2(SeO_3)$. The mother liquor was decanted from the crystals, which were then washed with water and methanol and allowed to dry. Crystals of **6** were manually separated from $UO_2(SeO_3)$. Yield, 191 mg (20% yield based on U). EDX analysis for $Pb(UO_2)(SeO_3)_2$ provided a Pb/U/Se ratio of 1:1:2. IR (KBr, cm^{-1}): ν(U═O, U−O, and Se═O) 883(s, sh), 857 (s), 846 (s), 831 (s), 789 (m), 709 (s), 660 (s, br).

Crystallographic Studies. Crystals of $Ag_2(UO_2)(SeO_3)_2$ (**1**), $K[(UO_2)(HSeO_3)(SeO_3)]$ (**2**), $Rb[(UO_2)(HSeO_3)(SeO_3)]$ (**3**), $Cs[(UO_2)(HSeO_3)(SeO_3)]$ (**4**), $Tl[(UO_2)(HSeO_3)(SeO_3)]$ (**5**), and $Pb(UO_2)(SeO_3)_2$ (**6**) were mounted on glass fibers and aligned on a Bruker SMART APEX CCD X-ray diffractometer. Intensity measurements were performed using graphite monochromated Mo Kα radiation from a sealed tube and a monocapillary. SMART was used for preliminary determination of the cell constants and data collection control. For all compounds, the intensities of reflections of a sphere were collected by a combination of 3 sets of exposures (frames). Each set had a different ϕ angle for the crystal, and each exposure covered a range of 0.3° in ω. A total of 1800 frames were collected with an exposure time per frame of 30 s.

For **1**−**6**, determinations of integral intensities and global cell refinement were performed with the Bruker SAINT (v 6.02) software package using a narrow-frame integration algorithm. A semiempirical absorption correction was applied on the basis of the intensities of symmetry-related reflections measured at different angular settings using SADABS.[27] Owing to the large absorption coefficients for **5** and **6**, face-indexed, analytical absorption corrections were applied in XPREP prior to SADABS corrections.[28] To accomplish this, individual shells of unmerged data were corrected analytically and exported in the same format. These files were subsequently treated by SADABS with a $\mu \cdot t$ parameter of 0. The program suite SHELXTL (v 5.1) was used for space group determination (XPREP), structure solution (XS), and refinement (XL).[29] In compounds **2**−**5**, the heavy atoms clearly dominate the X-ray scattering, making the resolution of the hydrogen positions for the $HSeO_3^-$ anions difficult and often unreliable. Only in **5** was the hydrogen atom located with a high degree of confidence. The final refinements included anisotropic displacement parameters for all atoms except hydrogen, and a secondary extinction parameter. Some crystallographic details are listed in Table 1 for **1**−**6**; additional details can be found in the Supporting Information.

Diffuse Reflectance Spectra. The diffuse reflectance spectrum of **6** was measured from 1800 to 200 nm using a Shimadzu UV3100 spectrophotometer equipped with an integrating sphere attachment. $BaSO_4$ was used as the standard. The Kubelka−Monk function was used to convert diffuse reflectance data to absorbance spectra.[30]

Secord-Order NLO Measurements. Powder SHG measurements on ungraded polycrystalline $Pb(UO_2)(SeO_3)_2$ (**6**) were performed on a modified Kurtz-NLO system using a 1064 nm light source.[31] No index matching fluid was used in the measurements. A detailed description of the apparatus has been published.[16]

Results and Discussion

Syntheses. The reactions of UO_3 with SeO_2 in the presence of $AgNO_3$, KCl, RbCl, CsCl, TlCl, or $Pb(NO_3)_2$ at 180 °C for 3 d in aqueous media results in the formation of $Ag_2(UO_2)(SeO_3)_2$ (**1**), $K[(UO_2)(HSeO_3)(SeO_3)]$ (**2**), $Rb[(UO_2)$-

(27) *SADABS*, program for absorption correction using SMART CCD based on the method of Blessing: Blessing, R. H. *Acta Crystallogr.* **1995**, *A51*, 33.
(28) Huang, F. Q.; Ibers, J. A. *Inorg. Chem.* **2001**, *40*, 2602.
(29) Sheldrick, G. M. *SHELXTL PC, Version 5.0, An Integrated System for Solving, Refining, and Displaying Crystal Structures from Diffraction Data*; Siemens Analytical X-ray Instruments, Inc.: Madison, WI,1994.
(30) Wendlandt, W. W.; Hecht, H. G. *Reflectance Spectroscopy*; Interscience Publishers: New York, 1966.
(31) Kurtz, S. K.; Perry, T. T. *J. Appl. Phys.* **1968**, *39*, 3798.

$(HSeO_3)(SeO_3)]$ (**3**), $Cs[(UO_2)(HSeO_3)(SeO_3)]$ (**4**), $Tl[(UO_2)(HSeO_3)(SeO_3)]$ (**5**), or $Pb(UO_2)(SeO_3)_2$ (**6**), respectively. The estimated pressure in these reactions is 11.5 atm. All of these reactions are straightforward, and reduction of the selenite anion to selenium is not observed. Clearly, the reactions of UO_3 and SeO_2 with additional metal ions are general routes to mixed-metal U(VI) compounds. However, in some cases, the yields of desired compounds are less than ideal, owing to the concomitant formation of uranyl selenite, $UO_2(SeO_3)$.[9] A similar observation was also made in the syntheses of alkali metal, alkaline-earth metal, main group, and transition metal uranyl iodate compounds, where the formation of $UO_2(IO_3)_2(H_2O)$ was ubiquitous.[1−4] We have not observed a rapid reaction of UO_3 with SeO_2 at room temperature.

Compounds **2**−**5** can be prepared in pure form in moderate to quantitative yields. However, we have been unable to prepare **1** and **6** without also forming $UO_2(SeO_3)$. Attempts were made to eliminate the formation of uranyl selenite by changing stoichiometry, scale, and water content (from 1 to 3 mL) and by increasing the temperature from 180 to 200 °C. Product mixtures were still obtained in the syntheses of **1** and **6**. Fortunately, $UO_2(SeO_3)$ can be easily manually separated from **1** and **6** owing to dramatic differences in crystal color and habit. For instance, compound **6** forms large orange clusters of crystals that can be separated from uranyl selenite with forceps. The synthesis of **6** reported in the Experimental Section is at twice the scale of the other reactions to allow for accurate determination of yield and for isolation of enough of the desired product to perform subsequent spectroscopic analyses. In general, our best crystallization results are obtained when less than 3 mL of water is employed in these reactions.

Structures. $Ag_2(UO_2)(SeO_3)_2$ (1), $K[(UO_2)(HSeO_3)(SeO_3)]$ (2), $Rb[(UO_2)(HSeO_3)(SeO_3)]$ (3), $Cs[(UO_2)(HSeO_3)(SeO_3)]$ (4), and $Tl[(UO_2)(HSeO_3)(SeO_3)]$ (5). The structures of **1**−**5** are all based upon similar two-dimensional $^2_\infty[(UO_2)(SeO_3)_2]^{2-}$ sheets that are separated by Ag^+, K^+, Rb^+, Cs^+, or Tl^+ cations, respectively, and will, therefore, be discussed together for the sake of brevity. The layers observed in **1** and in **2**−**5** have been previously observed in $[NH_4]_2[UO_2(SeO_3)_2]$[32] and $NH_4[UO_2(HSeO_3)(SeO_3)]$,[33] respectively. However, only **2**, **3**, and **5** are truly isostructural with $NH_4[UO_2(HSeO_3)(SeO_3)]$. Compound **4** actually has a *Z* value of 8 instead of 4 as found for the other compounds with this formula. In this compound, there are two crystallographically unique UO_2^{2+} centers, two SeO_3^{2-} anions, and two $HSeO_3^{1-}$ anions. Compound **1** is not isostructural with $[NH_4]_2[UO_2(SeO_3)_2]$ owing to substantial differences in the coordination requirements of the cations separating the layers.

The layers in **1**−**5** consist of uranyl, UO_2^{2+}, units that are coordinated by five selenite, SeO_3^{2-}, anions in the equatorial plane as shown in Figure 1. This creates UO_7 pentagonal bipyramidal coordination environments around the U(VI) centers, which is the most commonly observed geometry for hexavalent uranium in hydrothermal chemistry. The selenite

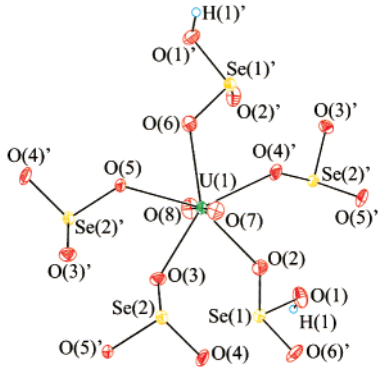

Figure 1. Fundamental building unit in $Ag_2(UO_2)(SeO_3)_2$ (**1**), $K[(UO_2)(HSeO_3)(SeO_3)]$ (**2**), $Rb[(UO_2)(HSeO_3)(SeO_3)]$ (**3**), $Cs[(UO_2)(HSeO_3)(SeO_3)]$ (**4**), and $Tl[(UO_2)(HSeO_3)(SeO_3)]$ (**5**) consisting of uranyl, UO_2^{2+}, cations coordinated by five bridging SeO_3^{2-} anions. 50% probability ellipsoids are depicted.

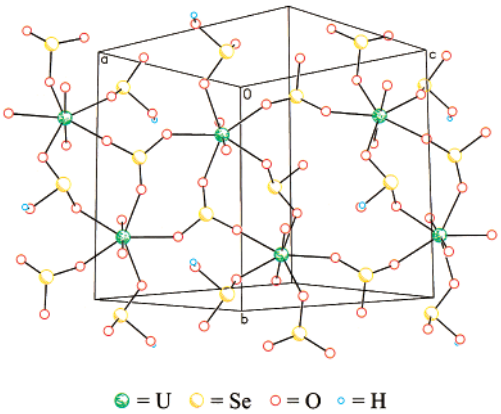

Figure 2. Two-dimensional uranyl selenite layers found in $Ag_2(UO_2)(SeO_3)_2$ (**1**), $K[(UO_2)(HSeO_3)(SeO_3)]$ (**2**), $Rb[(UO_2)(HSeO_3)(SeO_3)]$ (**3**), $Cs[(UO_2)(HSeO_3)(SeO_3)]$ (**4**), and $Tl[(UO_2)(HSeO_3)(SeO_3)]$ (**5**). In **1**, these layers are formulated as $^2_\infty[(UO_2)(SeO_3)_2]^{2-}$. In **2**−**5**, half of the selenite anions are protonated, yielding a layer composition of $^2_\infty[(UO_2)(HSeO_3)(SeO_3)]^{1-}$. The layer depicted is from **5** and shows the located hydrogen atom from the $HSeO_3^{1-}$ anion.

anions adopt bridging binding modes where they serve to link either two (Se(1)) or three (Se(2)) uranyl moieties and thereby create the two-dimensional networks observed in these compounds. The layers found in **5** are depicted in Figure 2 and are used to represent those also found in **1**−**4**. These layers can be compared to the anionic sheet topology[7] observed for $K_2[(UO_2)(MoO_4)]$[34] where one of the vertices of the MoO_4^{2-} tetrahedra is removed to yield the trigonal pyramids of SeO_3^{2-}.

Charge neutrality requirements require that half of the selenite anions in **2**−**5** be protonated to provide a layer composition of $^2_\infty[(UO_2)(HSeO_3)(SeO_3)]^{1-}$.[33] The protonation of these sites is probably due to the large size of the K^+, Rb^+, Cs^+, and Tl^+ cations, which cannot be packed close enough together to sufficiently balance localized charges within the layers. Fortunately, discerning the location of these protonated selenite anions is reasonably trivial. First, half of the selenite anions are triply bridging and can therefore not accommodate protons. The other selenite anions only

(32) Koshenlinna, M.; Mutikainen, I.; Leskelae, T.; Leskela, M. *Acta Chem. Scand.* **1997**, *51*, 264.
(33) Koshenlinna, M.; Valkonen, J. *Acta Crystallogr.* **1996**, *C52*, 1857.
(34) Sadikov, G. G.; Krasovskaya, T. I.; Polyakov, Y. A.; Nikolaev, V. P. *Inorg. Mater.* **1988**, *24*, 91.

Table 2. Se−O Bond Distances (Å) and Bond Valence Sum (BVS) Values for the Selenite Oxygen Atoms in $K[(UO_2)(HSeO_3)(SeO_3)]$ (**2**), $Rb[(UO_2)(HSeO_3)(SeO_3)]$ (**3**), $Cs[(UO_2)(HSeO_3)(SeO_3)]$ (**4**), and $Tl[(UO_2)(HSeO_3)(SeO_3)]$ (**5**)

$K[(UO_2)(HSeO_3)(SeO_3)]$ (**2**)			$Rb[(UO_2)(HSeO_3)(SeO_3)]$ (**3**)		
	distance	BVS		distance	BVS
Se(1)−O(1)	1.765(4)	1.13 (OH)	Se(1)−O(1)	1.768(4)	1.12 (OH)
Se(1)−O(2)	1.672(4)	1.98	Se(1)−O(2)	1.675(4)	1.98
Se(1)−O(6)	1.667(4)	1.98	Se(1)−O(6)	1.655(4)	2.02
Se(2)−O(3)	1.701(4)	1.93	Se(2)−O(3)	1.693(4)	1.94
Se(2)−O(4)	1.693(4)	1.93	Se(2)−O(4)	1.696(4)	1.92
Se(2)−O(5)	1.688(4)	1.87	Se(2)−O(5)	1.696(4)	1.85
$Cs[(UO_2)(HSeO_3)(SeO_3)]$ (**4**)			$Tl[(UO_2)(HSeO_3)(SeO_3)]$ (**5**)		
Se(1)−O(1)	1.747(4)	1.19 (OH)	Se(1)−O(1)	1.765(4)	1.13 (OH)
Se(1)−O(2)	1.654(4)	2.08	Se(1)−O(2)	1.670(4)	1.98
Se(1)−O(3)	1.670(4)	1.99	Se(1)−O(6)	1.672(4)	1.94
Se(2)−O(4)	1.776(4)	1.10 (OH)	Se(2)−O(3)	1.702(4)	1.89
Se(2)−O(5)	1.666(4)	1.99	Se(2)−O(4)	1.693(4)	1.92
Se(2)−O(6)	1.664(4)	2.00	Se(2)−O(5)	1.706(4)	1.80
Se(3)−O(7)	1.669(4)	2.01			
Se(3)−O(8)	1.688(4)	1.89			
Se(3)−O(9)	1.723(4)	1.82			
Se(4)−O(10)	1.698(4)	1.89			
Se(4)−O(11)	1.699(4)	1.87			
Se(4)−O(12)	1.696(4)	1.85			

bridge two uranyl centers and have one terminal oxo group. In compound **1**, for example, there is little variation in Se═O bond distance regardless of coordination mode, with Se═O bond distances ranging from 1.693(7) to 1.720(6) Å. In **4**, there are two crystallographically unique triply bridging selenite ligands and two unique anions that are doubly bridging. The former ligands have Se═O bond distances that range from 1.669(4) to 1.723(4) Å. The doubly bridging anions, however, have Se═O bond distances that range from 1.654(4) to 1.747(4) Å for Se(1) and from 1.664(4) to 1.776(4) Å for Se(2). In both cases, the longest distance is to the nominally terminal oxo atom.

On the basis of these data, we postulate that the longest Se−O bonds indicate the sites of protonation. In the case of **4**, the protonated oxygen atoms are O(1) and O(4). These arguments were used to predict the location of the hydrogen atoms in **2**−**5**, and from difference maps, the hydrogen atom was indeed observed in **5**. Further support for the formula assignments in these compounds are found in the bond valence sums for the U atoms in **1**−**5**, which have values that range from 5.90 to 5.97.[5,35,36] Se−O bond distances and bond valence sums for the selenite oxygen atoms in **2**−**5** are summarized in Table 2. These sums are consistent with the model we have proposed for the locations of the hydrogen atoms.

The final topic of discussion for compounds **1**−**5** is the coordination modes for the metal cations that serve to separate the uranyl selenite layers. In **2**−**5**, the K^+, Rb^+, Cs^+, and Tl^+ cations form only long ionic contacts with surrounding oxygen atoms, and therefore, these structures can be treated as two-dimensional. Compound **1**, however, cannot be treated as a truly low-dimensional compound because the selenite anions form strong covalent bonds with the Ag^+ cations. The cations, therefore, actually join the layers together to create a three-dimensional network structure, which is depicted in Figure 3. $Ag_2(UO_2)(SeO_3)_2$ contains two crystallographically unique silver atoms. Both silver atoms form distorted low-coordinate geometries. For Ag(1), there are two short Ag−O bonds of 2.292(8) and 2.269(7) Å and one long interaction of 2.578(7) Å forming an approximate trigonal planar environment. Ag(2) also resides in a distorted trigonal planar environment with three short Ag−O bonds ranging from 2.269(7) to 2.380(7) Å. However, there is an additional long Ag···O contact of 2.578(8) Å. Bond distances for **1**−**5** are available in the Supporting Information CIF files.

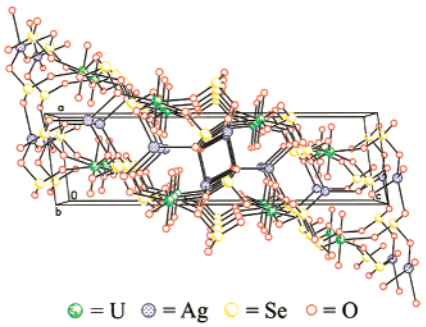

Figure 3. Three-dimensional network structure of $Ag_2(UO_2)(SeO_3)_2$ (**1**) showing $^2_\infty[(UO_2)(SeO_3)_2]^{2-}$ layers being joined by two crystallographically unique Ag^+ cations that form covalent bonds with the terminal oxo atoms from the selenite anions.

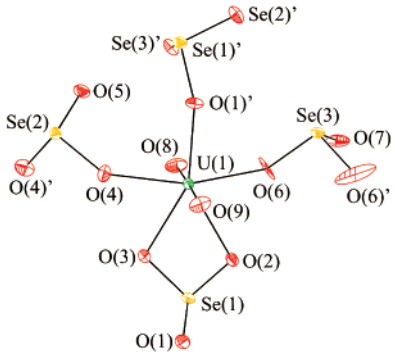

Figure 4. Fundamental building unit in $Pb(UO_2)(SeO_3)_2$ (**6**) consisting of uranyl, UO_2^{2+}, cations coordinated by three bridging SeO_3^{2-} anions that adopt both bridging and chelating/bridging binding modes. 50% probability ellipsoids are depicted.

$Pb(UO_2)(SeO_3)_2$ (6). The structure of **6** while still containing a two-dimensional uranyl selenite substructure is substantially different from that observed in **1**−**5**. The most important difference is the change in the manner in which the selenite anions coordinate the U(VI) centers. Here, instead of simply bridging uranyl moieties, the selenite ligands chelate *and* bridge between these centers, creating the fundamental building unit shown in Figure 4. However, as in **1**, the countercations cannot be neglected as they form short covalent bonds with both the terminal oxo groups from the selenite anions and the oxo group of the uranyl moieties. There are two crystallographically unique Pb^{2+} cations in **6**. Both of these cations are found in PbO_5 distorted square pyramidal coordination environments that indicate the presence of a stereochemically active lone pair of electrons. These polyhedra are shown in Figure 5. As expected, the bonds formed with the uranyl moieties are significantly longer than

(35) Brown, I. D.; Altermatt, D. *Acta Crystallogr.* **1985**, *B41*, 244.
(36) Brese, N. E.; O'Keeffe, M. *Acta Crystallogr.* **1991**, *B47*, 192.

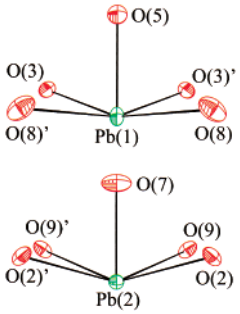

Figure 5. PbO_5 distorted square pyraminds in $Pb(UO_2)(SeO_3)_2$ (**6**). 50% probability ellipsoids are depicted.

Table 3. Selected Bond Distances (Å) for $Pb(UO_2)(SeO_3)_2$ (**6**)

Pb(1)—O(4)	2.368(5)	U(1)—O(9)	2.224(6)
Pb(1)—O(11)	2.388(8)	U(1)—O(12) (U═O)	1.794(6)
Pb(1)—O(12)	2.708(6) (×2)	U(1)—O(13) (U═O)	1.796(5)
Pb(2)—O(2)	2.439(5) (×2)	Se(1)—O(3)	1.704(5)
Pb(2)—O(5)	2.32(1)	Se(1)—O(11)	1.673(8) (×2)
Pb(2)—O(13)	2.683(5) (×2)	Se(2)—O(1)	1.689(5)
U(1)—O(1)	2.269(5)	Se(2)—O(2)	1.700(5)
U(1)—O(2)	2.461(5)	Se(2)—O(4)	1.721(5)
U(1)—O(3)	2.326(5)	Se(3)—O(5)	1.671(8)
U(1)—O(4)	2.431(5)	Se(3)—O(9)	1.691(7) (×2)

those with the selenite anions. The Pb—O bonds range from 2.32(1) to 2.439(5) Å for bonds to selenite and are 2.683(5) and 2.708(6) Å for interactions between the uranyl units and Pb^{2+}. Selected bond distances for **6** are given in Table 3. The bond valence sum for the U atom in **6** is 6.10.[5,35,36]

As indicated by the *Pmc*2_1 space group, $Pb(UO_2)(SeO_3)_2$ has a polar *c*-axis. Figure 6 demonstrates that the polarity in this structure is due to alignment of PbO_5 polyhedra and not the selenite anions. Therefore, the hydrothermal synthesis of **6** represents our first successful synthesis of a polar uranyl-containing compound that utilizes a C_{3v} ligand. This work is built upon the hypothesis of utilizing two different metal centers with stereochemically active lone pairs of electrons within a single compound to create polar structures.[13−16]

A key difference between the layers found in these uranyl selenites with those observed in uranyl iodates is the notable absence of μ_3-oxo or μ_3-hydroxo groups in the selenite compounds. This divergence in chemistry is most likely due to the differences in coordination ability of selenite versus iodate with the former probably being a better donor ligand. The preferential binding of iodate and selenite to the uranyl centers over competing anions present in these reactions, for example, chloride, is a reflection of the highly oxophilic nature of hexavalent uranium.[37,38]

Optical Properties of $Pb(UO_2)(SeO_3)_2$ (6). The optical properties of **6** were examined in detail to explore potential uses of this compound as a nonlinear optical material given its crystallization in a polar space group. The diffuse reflectance spectrum of **6**, shown in Figure 7, is quite interesting. First, there are two optical transitions at approximately 330 and 440 nm. The transition at 440 nm

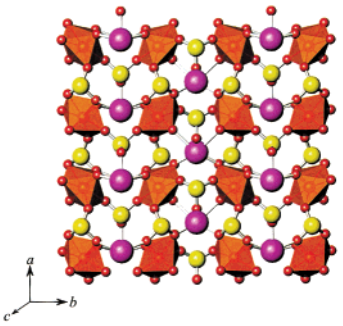

Figure 6. Alignment of the PbO_5 distorted square pyraminds along the *c*-axis in $Pb(UO_2)(SeO_3)_2$ (**6**).

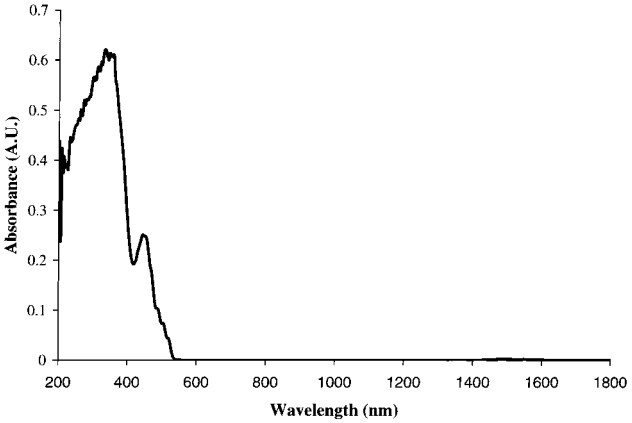

Figure 7. Diffuse reflectance spectrum of $Pb(UO_2)(SeO_3)_2$ (**6**) showing absorption bands at 330 and 440 nm. Both of these transitions show fine structure, and the latter is responsible for the orange coloration of **6**.

contains fine structure with 16 cm^{-1} separations between vibronic transitions. The transition at 330 nm also contains fine structure, but these transitions are more difficult to resolve from one another. It is well-known that most uranyl-containing compounds emit green light when irradiated with long wavelength UV light.[38,39] These transitions have been completely assigned in $Cs_2UO_2Cl_4$ by Denning et al.[39] It is, therefore, reasonable to speculate that this transition is due to absorption by the uranyl centers. The second transition at 440 nm, which tails off to approximately 530 nm, is responsible for the orange coloration of **6**.

For analyzing the SHG response, the fact that **6** does not absorb light to an appreciable degree at 1064 or 532 nm is important. Therefore, second-harmonic generation (SHG) measurements were performed on **6** using a modified Kurtz-NLO system with a 1064 nm light source on powders ground from crystals of **6**. Generation of SHG light of 532 nm was carefully measured, and these studies indicated a small response of 5× α-quartz. Even though this response is quite small, these measurements do confirm our assignment of **6** in a noncentrosymmetric space group.

Conclusions

In this study, we have demonstrated the viability of the selenite anion for use in the syntheses of mixed-metal and

(37) Weigel, F. In *The Chemistry of the Actinide Elements*; Katz, J. J., Seaborg, G. T., Morss, J. R., Eds.; Chapman and Hall: London, 1986; Chapter 5.
(38) Carnall, W. T.; Crosswhite, H. M. In *The Chemistry of the Actinide Elements*; Katz, J. J., Seaborg, G. T., Morss, J. R., Eds.; Chapman and Hall: London, 1986; Chapter 16.
(39) Denning, R. G.; Norris, J. O. W.; Short, I. G.; Snellgrove, T. R.; Woodwark, D. R. In *Lanthanide and Actinide Chemistry and Spectroscopy*; Edelstein, N. M., Ed.; ACS Symposium Series 131; American Chemical Society: Washington, DC, 1980; Chapter 15.

low-dimensional uranium phases. These studies further show that selenite has a strong tendency for forming covalent bonds with Pb^{2+}, which was not observed in uranyl iodate chemistry.[3] The use of a second metal center with a stereochemically active lone pair of electrons has indeed proven to be the solution to the successful synthesis of a polar uranyl-containing compound where C_{3v} anions are utilized in the construction of extended structures.

Acknowledgment. T.E.A.-S. acknowledges NASA (ASGC) and the Department of Energy, Heavy Elements Program (Grant DE-FG02-01ER15187) for support of this work. T.E.A.-S. acknowledges P. Shiv Halasyamani (University of Houston) for the SHG measurements. The authors also wish to thank Mutlu Kartin (Clemson University) for assistance in obtaining the diffuse reflectance spectrum of **6**.

Supporting Information Available: X-ray crystallographic files for $Ag_2(UO_2)(SeO_3)_2$ (**1**), $K[(UO_2)(HSeO_3)(SeO_3)]$ (**2**), $Rb[(UO_2)(HSeO_3)(SeO_3)]$ (**3**), $Cs[(UO_2)(HSeO_3)(SeO_3)]$ (**4**), $Tl[(UO_2)(HSeO_3)(SeO_3)]$ (**5**), or $Pb(UO_2)(SeO_3)_2$ (**6**) in CIF format. This material is available free of charge via the Internet at http://pubs.acs.org.

IC0110732